The Danish Meteorological Institute

DMI Report 21-22. Snow and Ice Thickness from Model and Remote Sensing

Final scientific report of the 2020 National Centre for Climate Research Work Package 1.2.4, Ice thickness – Version 1.2.

DMI Report
15 January 2021

By Gorm Dybkjær*, Imke Sievers*, Hoyeon Shi**, Jens Murawski*, Vasily Korabel*, Till Rasmussen*, Rasmus Tonboe*;
*DMI, **SNU

Danmarks Meteorologiske Institut

Colophon

Serial title	DMI Report
Title	DMI Report 21-22. Snow and Ice Thickness from Model and Remote Sensing
Subtitle	Final scientific report of the 2020 National Centre for Climate Research Work Package 1.2.4, Ice thickness – Version 1.2.
Author(s)	Gorm Dybkjær*, Imke Sievers*, Hoyeon Shi**, Jens Murawski*, Vasily Korabel*, Till Rasmussen*, Rasmus Tonboe*; *DMI, **SNU
Other contributors	Professor Byung-Ju Sohn, Seoul National University
Responsible institution	Danish Meteorological Institute, DMI
Language	English
Keywords	Arctic, Cryosphere, sea ice thickness, snow thickness, Remote Sensing, modelling, time series analysis.
URL	https://www.dmi.dk/publikationer/
Digital ISBN	978-87-7478-696-2
ISSN	2445-9127
Version	15 January 2021
Website	www.dmi.dk
Copyright	DMI

Danmarks Meteorologiske Institut

Content

1 Abstract

This study compares snow and ice thickness from two independent sources in the period from 2003 to 2015. The snow and ice data are obtained from an ocean and sea ice model and from satellite measurements of the sea ice temperature profile and its freeboard
Both the model and the observations consistently show that the Arctic sea ice is thinning in most regions and throughout the season during the 13 years. However, the model and the observations disagree in the rate of thinning, and the mismatch is dependent on the geographical regime and on the time of year. Moreover, the ice thickness distribution in the observation data is much wider than the modelled ice thickness distribution.

Model results and observations also disagree in snow thickness trends during the 13 years depending on region and season. However, model and observations largely agree in mean snow depth distribution.

2 Resumé

Dette studie har sammenlignet is- og snetykkelser i perioden fra 2003 til 2015 fra 2 uafhængige kilder, nemlig fra modelberegninger og fra satellitobservationer af isens temperatur profil og dens fribord.

Modelberegninger og observationer viser stort set samstemmende, at størstedelen af den Arktiske havis bliver tyndere år for år og over hele året. De to uafhængige metoder er uenige om den hastighed hvormed udtyndingen af den arktiske havis sker, afhængig af hvilke områder af Arktis der er I fokus. Desuden er den modellerede istykkelsesfordeling meget smallere end den observerede.

De 2 metoder viser ofte temmelig forskellige trends i snetykkelses fordelingen, afhængig af tid og sted. Modelberegninger og observationer er meget enige om det samlede snefald i Arktis og den statistiske snetykkelses distribution.

3 Introduction

The Danish National Centre for Climate Research (Nationalt Center for Klimaforskning, NCKF) has been a source of funding for the Danish Meteorological Institute and collaborators for climate change related research during 2020. 18 work packages (WPs) under the NCKF-2020 are divided under 4 general themes:

1. Arctic and Antarctic Research
2. Climate change in the near future
3. Use of climate data
4. Support for the IPCC

This WP 1.2.4 “Ice Thickness” is concerned with the use of climate data in Arctic research and climate change in recent years (theme 3).

The Arctic sea ice and snow thickness has a strong influence on the climate on the Northern Hemisphere (NH) and hence, the on-going changes in the Arctic sea ice influence the future weather and climate on the NH in general.

In this WP we produce and analyse two independent data sets of snow and sea ice thickness in the Arctic, covering the period 2003 to 2015. By comparing data from a physical model setup with independent observation we wish to identify strength and weaknesses of both data sets in order to improve the model to predict the future Arctic climate and to strengthen the reliability of such climate predictions.

The modelled snow and ice thickness data are produced by a coupled ocean and ice model (henceforth “model” data) and the other snow and ice data are based on satellite observations (henceforth “observation” data).

3.1 Introduction to Model data

Modelled sea ice data from a coupled NEMO 4 (Madec et al) – CICE6 (Hunke et al., 2021) model run have been analyzed in order to identify trends in the arctic sea ice and snow thickness. The time period covers the 13 years from 2003 to 2015. The aim is to inter-compare the modeled trends with observed ones, that have been derived from remotely sensed data and to analyze the capabilities of both, models and satellites in order to detect comparable trends. For this, the results of the NEMO4-CICE6 free run, without data assimilation were converted to a grid that is matching with satellite data. Only sea ice thickness in grid cells with concentration larger than 95% was applied analyzed, in order to comply with the detection limits of the satellite algorithm..

The statistical significance has been analyzed as a function of the spatial and temporal coverage of the data set. The results are identical for sea ice thickness and snow thickness, which is likely to be a consequence of the relatively high minimum-concentration-value that has been chosen. All the ice covered points are snow covered as well. Here, we present only one curve, which represents both data sets. For nearly all month, 95% of the area is covered by a data set that covers at least 2 years. Only 5% of the area is covered by only 1 year. The only month that requires a 3 years data set to cover 5% of the total ice covered area is November. On the other hand, most of the ice covered area: 79.4% is experiencing ice coverage at all years between 2003 and 2015. We have chosen to use a minimum length of the data set of 6 years for the analysis. This corresponds to little less than 90% of the total ice covered area. Statistics of the data sets are shown in Figure 1.

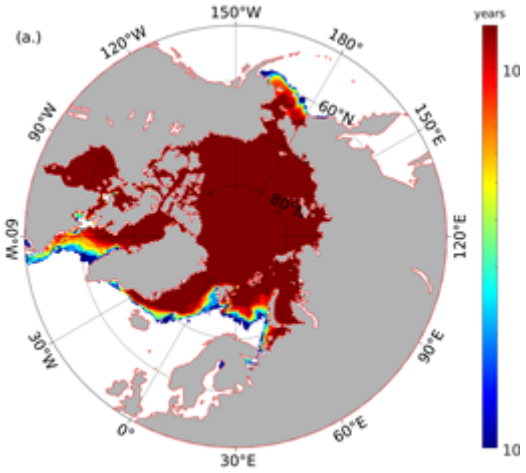

Figure 1 Spatial coverage of the data set. Number of years between 2003 and 2015 with modeled ice concentration of at least 95% in March.

3.2 Introduction to the remote sensing data

The Arctic sea ice thickness and the snow depth is important for assessment of the Arctic climate change and satellite altimeters have been used for estimating sea ice thickness for nearly two decades (Laxon et al., 2003; Kwok et al., 2009; Laxon et al., 2013). The altimeters measure the sea ice freeboard, which is converted to sea ice thickness with assumptions, about the snow depth, snow/ice densities, and radar penetration (Ricker et al., 2014). We hereafter refer to this procedure as the 'freeboard–thickness conversion'.

Generally, there are two types of satellite altimeters measuring different sea ice freeboards: (1) lidar altimeters such as NASA's ICESat (Zwally et al., 2002) mission which is measuring the total freeboard (F_t), the height from the sea surface in leads, to the snow surface; (2) radar altimeters such as ESA's CryoSat-2 (CS2) (Wingham et al., 2006) that measures the radar freeboard (F_r), the difference in the radar ranging between the sea surface and the radar scattering horizon. By applying two correction terms regarding the wave propagation speed change in the snow layer (F_c) and the displacement of the scattering horizon from the ice surface (F_p), the radar freeboard is converted to the ice freeboard (F_i): the height from the sea surface to the snow–ice interface (F_i).

For both lidar and radar altimeters, snow depth (h_s) is required as an input to constrain the freeboard–thickness conversion; thus, the conversion results are dependent on the snow depth (Ricker et al., 2014; Kern et al. 2015). According to Zygmuntowska et al. (2014), up to 70% of uncertainty in the freeboard–thickness conversion stems from the poorly constrained snow depth. However, mapping the pan-Arctic snow depth distribution is challenging.

The most commonly used snow depth information for the freeboard–thickness conversion is the modified version of the snow depth climatology by Warren et al. (1999) (hereafter W99). W99 is based on in-situ measurements at Soviet drifting stations (1954–1991) mostly on multi-year ice (MYI). Kurtz and Farrell (2011) compared W99 with Operation IceBridge (OIB) snow depth measurements in 2009 and reported that W99 is still valid in the MYI region, but significantly differed from OIB snow depth on first-year ice (FYI). Based on that study, Modified W99 (hereafter MW99) was developed, which halves W99 snow depth in regions covered by FYI.

However, the use of MW99 for the freeboard to thickness conversion understandably yields a substantial error, considering that W99 is a climatology which cannot be treated as the actual snow depth. Especially, Kim et al. (2020) revealed that the use of MW99 results in the systematic bias between the ice thickness from ICESat and CryoSat-2 of approximately 50 cm, making the construction of consistent ice thickness

records from those two altimeters difficult. Therefore, it should be beneficial if MW99 is replaced with real snow depth to obtain the combined ice thickness record.

Recently, Shi et al. (2020) estimated snow depth and ice thickness simultaneously by constraining the freeboard to thickness conversion with the ratio of snow depth to ice thickness (referred to as α) rather than snow depth. α was empirically determined from satellite-derived air-snow interface temperature (T_{as}) and snow–ice interface temperature (T_{si}). An evaluation using NASA's Operation IceBridge measurements of snow and ice thickness showed improvement on mean bias of ice thickness estimation.

Extending Shi et al. (2020) results, this study aims to construct the snow depth and ice thickness record from ICESat and CS2 freeboard measurements. Datasets, methodology, and preliminary results of trend analysis of ice and snow thickness are included below.

4 Methodology

The applied methodologies used to estimate Arctic snow and sea ice thickness are independent and conceptually different. The model set-up generates data based on physical models forced by atmospheric model data and the remote sensing technique is constrained by basic thermodynamically processes and an equilibrium temperature profile from satellite derived snow skin and ice/snow and standard water/ice interface temperatures.

In the following the two methods are described separately as the “remote sensing” and the “model” methodology.

4.1 Remote Sensing methodology

The remote sensing methodology applied for this analysis is a novel method that derives snow and ice thickness simultaneously. For that reason the method is described in some detail here. A thorough description of the methodology is also given by Shi et al. (2020). Here we have applied the method for the month of February, March and November 2003-2015.

4.1.1 Calculation of α from satellite derived temperatures

The α-*parameter* is defined as the ratio of snow depth (h_s) and sea ice thickness (H_i), Eq 1.

$$\alpha = h_s/H_i \qquad (1)$$

Here the α is estimated from the T_{as} and T_{si} by using the α-prediction equation in Shi et al. (2020). The α-prediction equation is an empirical relationship between α and the ratio of temperature difference of the snow layer to the difference of the ice layer. For monthly temperature data, the α-prediction equation is:

$$\alpha = \begin{cases} 0.185\frac{\Delta T_{snow}}{\Delta T_{ice}} + 0.022 & \frac{\Delta T_{snow}}{\Delta T_{ice}} \leq 1.769 \\ 0.076\frac{\Delta T_{snow}}{\Delta T_{ice}} + 0.214 & \frac{\Delta T_{snow}}{\Delta T_{ice}} > 1.769 \end{cases} \qquad (2)$$

Here, ΔT denotes the temperature difference between the top and bottom of each of the snow and ice layers (i.e. $\Delta T_{snow} = T_{as} - T_{si}$, $\Delta T_{ice} = T_{si} - T_{iw}$). T_{iw} is the ice-water interface temperature which is constant at -1.5 °C. α values are calculated only at those pixels where the mean monthly sea ice concentration (SIC) is greater than 95% and rejected if T_{as} is warmer than T_{si}.

4.1.2 Simultaneous retrieval of ice thickness and snow depth using α

Here, we describe how α constrains the freeboard - thickness conversion and, as a result, yields both ice thickness and snow depth. Based on the assumed hydrostatic balance, ice thickness can be obtained from total freeboard or radar freeboard as follows (Shi et al., 2020):

$$H_i = \frac{\rho_w}{\rho_w - \rho_i} F_t - \frac{\rho_w - \rho_s}{\rho_w - \rho_i} h_s \qquad (3)$$

$$H_i = \frac{\rho_w}{\rho_w - \rho_i} F_r + \frac{(f\eta_s - 1)\rho_w + \rho_s}{\rho_w - \rho_i} h_s \qquad (4)$$

Here, ρ_w, ρ_i, and ρ_s denote the bulk densities of water, ice, and snow layer, respectively. *f* denotes the radar penetration factor (Armitage and Ridout, 2015), which is the depth of the radar scattering horizon relative to the snow depth (e.g. *f* = 1 if the radar scattering horizon is at the snow–ice interface and *f* = 0 if the radar scattering horizon is at air-snow interface). Substituting h_s in Eqs. (3) and (4) with αH_i yields the following equations.

$$H_i = \frac{\rho_w}{\rho_w - \rho_i + \alpha(\rho_w - \rho_s)} F_t \qquad (5)$$

$$H_i = \frac{\rho_w}{\rho_w - \rho_i - \alpha\{(f\eta_s - 1)\rho_w + \rho_s\}} F_r \qquad (6)$$

From Eqs. (1), (5) and (6), it is evident that the snow depth and ice thickness can be simultaneously estimated from the freeboards and α, once ρ, f and η_s are known.

The densities are prescribed with those used for the OIB data processing: ρ_s, ρ_i, and ρ_w are 0.320 g cm^{-3}, 0.915 g cm^{-3}, and 1.024 g cm^{-3}, respectively (Kurtz et al., 2013). Radar penetration factor f is set to be 0.84 for CS2 (Armitage and Ridout, 2015) and η_s is parameterized as a function of the snow density, i.e., η_s $=(1+0.51\rho_s)^{1.5}$ (Ulaby et al., 1986). In solving Eq. (6), cases showing negative ice thickness ($\alpha \geq 0.291$ for the given densities and radar penetration factor) are rejected.

4.2 Model methodology

The modelled snow thickness, sea ice thickness freeboard and surface temperature are calculated by a coupled model framework including NEMO v4 (Gurvan et al., 2019) and CICE v6 (CICE, 2021). The model runs on a 10x10km Arctic grid with 75 ocean levels and 7 ice levels in 5 categories as well as one snow layer. The coupling frequency is 600 seconds. The simulation started in 1987 and here we use data from 2003-2015. The initial conditions for the ocean are from the ORAS5 ocean reanalysis (Zuo et al 2019). The sea ice initial conditions are calculated from sea surface temperatures below freezing point in the initial ocean conditions and are set to 2m accordingly. CICEs options for melt ponds, land fast ice, mushy-layer thermodynamics are turned on. The sea ice rheology is calculated following the elastic-viscous-plastic (EVP) model (Hunke and Dukovicz, 1997)
The atmospheric surface forcing consists of DFS5.2 (Dussin et al., 2016) forcing and the lateral boundaries are forced with monthly GLORYS12 data (GLORYS, 2021).

Model parameters used in this study are:

- Snow in meter: Snow is accumulated on ice throughout the winter season depending on the precipitation and atmospheric temperature. If the snow layer starts below sea surface some of the snowpack is flooded and converted into ice. No processes relocating the snow on the ice are considered.
- Sea Ice Thickness in meter: The variable used in this study is the grid cell mean ice thickness. Each grid cell is divided into 5 thickness categories (plus open water). Each of the 5 categories is divided into seven vertical layers. Each category covers a certain percentage of the cell and has an upper and lower thickness bound. The weighted mean is the used sea ice thickness here.
- Surface Temperature in Kelvin: Temperature at ice/snow-atmosphere interface. It never raises over 0°C.
- Freeboard: CICE calculates snow freeboard as the sum of snow and ice thickness minus the ice draft, per ice area.

All parameters were interpolated onto the satellite products grid using CDO.

5 Data

The input data sets to the model and satellite observation set-ups are independent. The satellite observation data are derived from satellite measurements of the snow and ice temperature profile and freeboard and the model data are derived from physical models forced by data from atmospheric models. These data sets are subsequently denoted “satellite” and “model”, respectively.

Data are here referred to as RS input data and Model input data.

5.1 Satellite input data

Several data sets are used for the remote sensing methodology. Beside satellite input data sets, observations from Ice Mass balance Buoys (IMB) are used to derive the –coefficients in equation 2. The applied IMB are compiled in an in situ data base hosted by DMI through the EUMETSAT OSISAF project. Most of the IMB data are provided by CRRELL buoys (CRREL, 2021).

5.1.1 Satellite-derived temperatures

To obtain α over the Arctic Ocean, satellite-derived T_{as} and T_{si} data are required. T_{as} is obtained from Arctic and Antarctic ice Surface Temperatures from thermal Infrared satellites sensors – version 2 (AASTI-v2) data (Dybkjær et al., 2020). AASTI T_{as} is derived from CM SAF cLoud, Albedo and surface Radiation dataset from AVHRR data - Edition 2 (CLARA-A2) dataset (Karlsson et al., 2017), based on the algorithm described in Dybkjær et al. (2018). Information on the validation of this product is found in Dybkjær and Eastwood (2016). Monthly AASTI-v2 data in a 0.25° grid format are re-gridded in a 25 km Polar Stereographic SSM/I Grid.

T_{si} is obtained from 6.9 GHz brightness temperature (TB) measurements based on the algorithm of Lee and Sohn (2015). To do so, level 3 monthly ascending/descending TBs of Advanced Microwave Scanning Radiometer for EOS (AMSR-E) and AMSR-2 are used. The averages of ascending and descending data are used for estimating T_{si}. In case of AMSR-2 TB, it is adjusted to AMSR-E TB according to inter-calibration result of JAXA (2015). The data are in the 25 km grid format (daily mean).

5.1.2 Satellite freeboard data

For examining the ice thickness and snow depth over the Arctic Ocean, satellite sea ice freeboard data are required. To do so, ICESat total freeboard data during 2003-2008 period and CS2 radar freeboard data during 2010-2015 period are used.

ICESat total freeboard data are obtained from the National Snow and Ice Data Center (NSIDC). The ICESat observation cycle was approximately three months each year, mainly the periods from February–March (FM), May– June (MJ), and October–November (ON), and the temporal coverage varied each year. Detailed descriptions on the ICESat data can be found in Yi and Zwally (2009). In this study, track data for each month (November, February, March, and April) are collocated on the 25 km grid to produce monthly total freeboard.

To obtain CS2 radar freeboard data, CS2 freeboard measurement summary data distributed by NSIDC are used (Kurtz and Harbeck, 2017). They are monthly mean composites of CS2 ice freeboard data in the 25 km grid format, covering the entire Arctic, and available from September 2010. Detailed descriptions of the re-tracker algorithm used in this dataset are found in the study by Kurtz et al. (2014). The dataset also includes MW99 (h_s^{MW99}) and W99 snow density climatology used for producing the ice freeboard.

The NSIDC CS2 ice freeboard data (F_i^{CS2}) assumed that the radar scattering horizon is at the snow–ice interface and applied a wave propagation speed correction which is not wanted in our processing. However, the correction was made using h_s^{MW99} and W99 snow density climatology with an erroneous form of $h_c = (1 - \eta_s^{-1})\, h_s$, instead of the proper form of $h_c = (\eta_s - 1)\, h_s$ (Mallett et al., 2020), where η_s is the refractive index of the snow layer. Thus, it is straightforward to derive the CS2 radar freeboard by removing the correction term as in the following equation (Eq. 7).

$$F_r^{CS2} = F_i^{CS2} - (1 - \eta_s^{-1}) h_s^{MW99} \quad (7)$$

Here, η_s is parameterized as a function of the snow density, i.e. $\eta_s = (1 + 1.7\rho_s + 0.7\rho_s^2)^{0.5}$ (Tiuri et al., 1984), and ρ_s is taken from the W99 climatology, after Kurtz and Harbeck (2017).

5.1.3 Sea ice concentration

Calculation of α is done for those pixels where the monthly SIC is greater than 95%. To determine pixels that meet this SIC criterion, 'NOAA/NSIDC Climate Data Record of Passive Microwave Sea Ice Concentration - Version 3' produced by Meier et al. (2017) is used. This monthly SIC dataset is provided in the 25 km grid format.

5.2 Model input data

The model is forced every 3rdh by 2m Atmospheric temperature, 10m u-, v-wind speed, humidity, and every 24th h by total precipitation, snow, and downward short and long wave radiation. The data used is the DFS5.2 forcing which is a modified ERA-Interim forcing set. The main correction over the Arctic is a temperature and humidity correction towards the POLES climatology (Rigor et al., 2000) as described by Dussin et al. (2016).
The lateral boundaries are forced with monthly baroclinic and barotropic velocity fields as well as salinity, temperature and sea surface height fields from the GLORYS12 ocean reanalysis. The boundaries are chosen so that no sea ice boundary conditions are needed.

Fresh water input from rivers is distributed over the upper 15 meter according to a river mouth mask distributing fresh water on a monthly basis from river climatology. Tidal forcing comes from the TPXO tidal model. Salinity and Temperature initial fields are climatology calculated from the ORAS5 Ocean reanalysis.

6 Results

The snow and ice thickness estimates from model and observations are presented and compared in different ways. Absolute values of snow and ice thickness are presented in time series for inter-comparison of the two methods and to compare with results from the literature. Trends of each parameter are also inter-compared and put in context of results from the literature. Finally, the geographical and statistical distributions of snow and ice thicknesses are compared to evaluate the qualitative agreement between the two methods, i.e. to evaluate if the geographical patterns look alike and if the statistical mean and standard deviation are comparable.

The results are further stratified into sea ice domains in order to analyse differences between e.g. First Year Ice and Multi Year Ice (FYI and MYI). The arctic is divided into predominantly FYI (eastern Arctic) and predominantly MYI (western Arctic) as guided by OSISAF ice types data (OSISAF, 2020). Figure 2 show the two areas marked in blue. Also a division into the area north of latitude 80 N is included. This area represents an area of permanent dense ice coverage with mixed multi-year and seasonal ice coverage. Finally, results from the entire Arctic region are included.

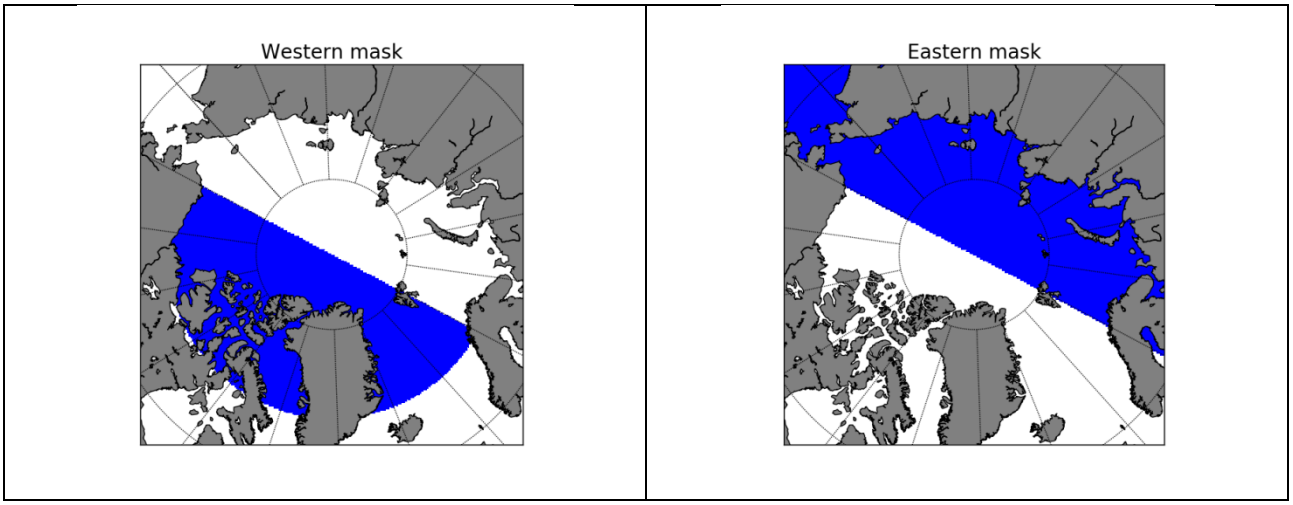

Figure 2 Area masks for western (left panel) and eastern (right panel) Arctic used for stratified analysis into areas dominated by MYI and FYO, respectively.

6.1 Freeboard

Freeboard estimates from the model are crucial for the models conception of the state of snow and sea ice. Likewise, the freeboard estimated from satellite is crucial for the observational method to estimate sensible snow and ice thickness. An agreement between model and satellite freeboard magnitude is a condition for the two methods to produce comparable snow and ice thickness estimates.
The ice freeboards from both ICESat and CryoSat for the eastern and western Arctic are compared to modelled freeboards in Figure 3.
In both figures the model freeboard shows growth throughout the winter while the Satellite data show less variability, and not necessarily constant growth throughout the winter. The observed freeboards are generally larger than the model estimates. The model loses almost all ice throughout the summer which can explain the higher freeboard growth throughout the winter compared to the satellite data. There is a higher agreement in eastern Arctic freeboard comparison especially for the ICESat period. Since the model almost melts all MYI, this might be explained with the western side being predominantly MYI ice while the eastern Arctic is dominated by FYI. Future model simulations should look into adjusting albedo values to get more realistic MYI areas in the model.

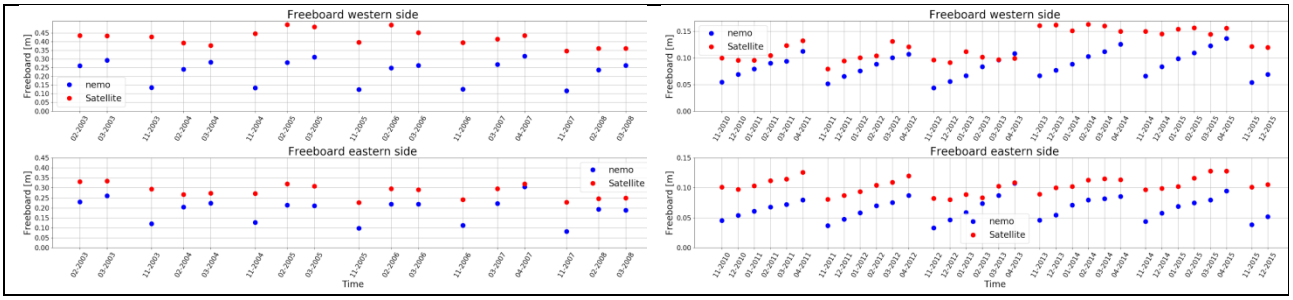

Figure 3 Ice freeboard from model and IceSat (left column) and CryoSat (right column) in the western Arctic (top row) and eastern Arctic (bottom row). Model freeboards are indicated with blue dots and satellite freeboard with red dots

6.2 Snow and ice thickness time series

All observed and modelled snow depth and ice thickness data for the mixed ice domain north of latitude 80 N are plotted in Figure 4 as time series. Both snow depth estimates are within approximately the same range, but occasionally negatively correlated inter-annually. The model simply accumulates the snow that falls during the winter season, whereas the observed snow depth does not necessarily increase in the period of a winter. Both estimates are realistic scenarios.

The modelled ice thickness is in general lower than the satellite retrieved ice thickness. The modelled ice thickness increases steadily during the winter month. The November starting point of the modelled ice thickness is between 0.5 and 1.0 meter. That is an unrealistically low for that part of the Arctic Ocean in the period of interest, and it is by others estimated to be more than 2 meters (Kwok and Rothrock, 2009b).

Another interesting difference between modelled and observed ice thickness is the changes over time or lack of change. The modelled thickness trend is nearly zero, where the trend of observed ice thickness is clearly negative – at least until 2013. The observed negative trend is very much in line with other observations in the central Arctic (Kwok, 2018; Lindsay and Schweiger, 2015). This is also elaborated below.

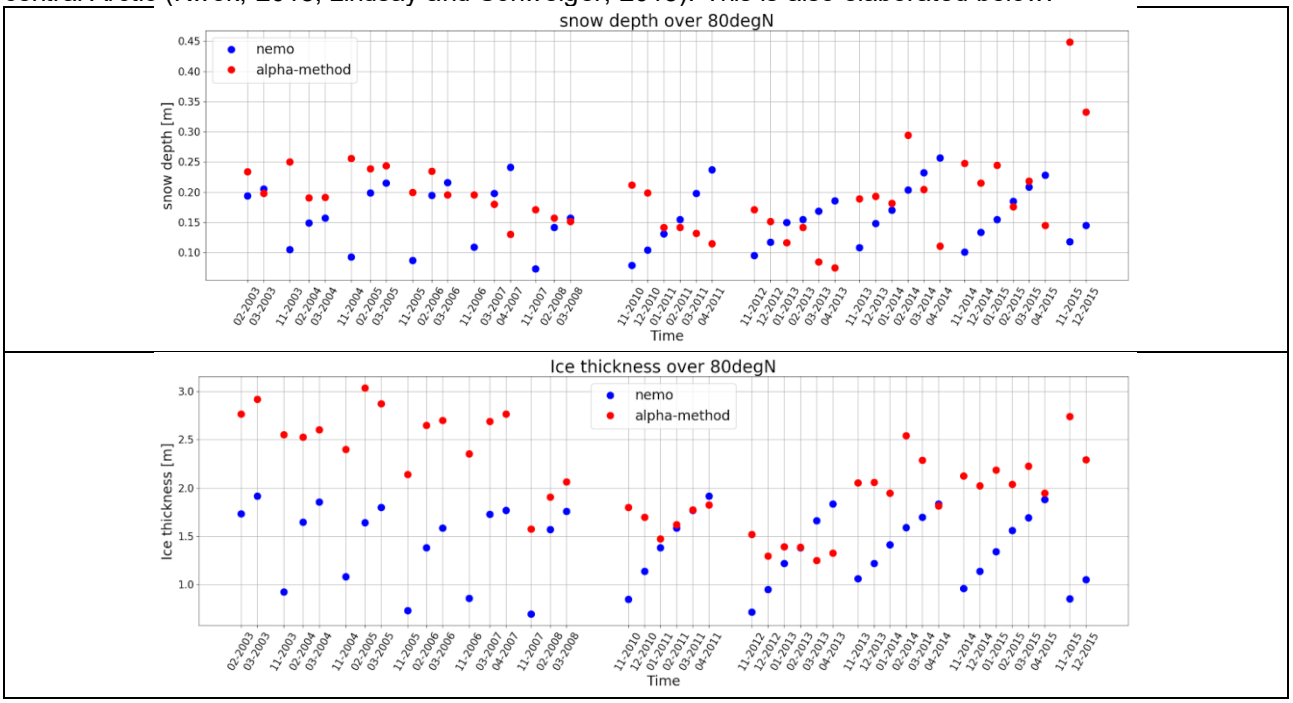

Figure 4 Snow depths (top) and ice thickness (bottom) in the mixed MYI/FYI ice domains north of latitude 80 N.

6.3 Trends of Ice and Snow thickness

Linear trend for modelled and observed sea ice thickness and snow depth has been calculated for three month of the year, namely February, March and November. These months are the three most consistently covered months in the data set.

The data set is stratifying into characteristic ice domains, namely: 1) the area north of latitude 80 N (+80N), 2 and 3) the Western (West) and Eastern Arctic (East) (Figure 2) and finally 4) the entire Arctic domain (EA). These areas represent a permanent closed ice region with mixed MYI and FYI, predominantly MYI and FYI and finally the full Arctic ice domain, respectively. All data points that are not covered by observations are excluded, to make the modelled and observed time series comparable. All trend results are summarized in Table 1. Results winter month, February and March, are presented as full data set time series with trend lines for EA, West and East domains in Figure 5, Figure 6 and Figure 7.

Table 1 Trends in modelled (Mod) and observed (Obs) sea ice thickness and (SIT) and snow depth (SD) for the entire arctic (EA), the area north of latitude 80 N (+80N), the eastern arctic with predominantly FYI (East) and the western Arctic with predominantly MYI (West), for the period 2003-2015.

Period 2003-2015	Month	SIT Obs [cm/y]	SIT Mod [cm/y]	SD Obs [mm/y]	SD Mod [mm/y]
+80N	Febuary	-8.01	-1.23	-4.2	0.327
EA		-7.14	-1.15	-4.6	0.133
East		-9.56	-0.88	-4.7	-0.364
West		-4.53	-1.53	-4.4	0.832
N80	March	-8.97	-1.32	-4.1	1.7
EA		-8.34	-1.34	-3.7	1.2
East		-11.91	-1.32	-5.1	0.689
West		-4.42	-1.38	-2.1	1.9
N80	November	-1.11	0.11	6.0	0.961
EA		-2.77	-0.12	1.2	0.333

Period 2003-2015	Month	SIT Obs [cm/y]	SIT Mod [cm/y]	SD Obs [mm/y]	SD Mod [mm/y]
East		-3.07	-0.40	4.5	-0.013
West		-0.57	0.21	3.4	0.741

The general pattern for modelled and observed sea ice thickness changes from 2003 to 2015 is a general thinning of the Arctic sea ice in the analysed regions. The thinning is stronger during winter than in November. This pattern is in agreement with other studies of which some document thinning of the Arctic sea ice since the 1980'ies (Kwok and Rothrock, 2009b; Kwok, 2018; Lindsay et al., 2009; Lindsay and Schweiger, 2015). Lindsay and Schweiger (2015) estimated the thinning trend for Arctic basin ice thickness to be -0.58 m/decade from 2000-2012. The corresponding trend from observation data in this study is 0.71 m/decade, provided that the mean of March and November trends is representative for annual ice thickness trend.

The observed trends are consistently most negative in February, March and November in the Eastern Arctic which is dominated by FYI and least negative in the Western Arctic where MYI is dominating. That can be explained by increasing areas and periods of open water in the Eastern arctic (Goldstein et al., 2018), resulting in strong positive water temperature anomalies in recent decades. The general thinning is also reflected in the general younger ice age in the Arctic Ocean, with a particular high rate of rejuvenation in the East Siberian Sea (Maslanik et al., 2011).

In contrast to the observed ice thickness trends, the modelled trends are very low negative, generally around -1 cm/y. That does not comply with the observation data in this study and in the numbers from the literature (Kwok and Rothrock, 2009b; Kwok, 2018; Lindsay et al., 2009; Lindsay and Schweiger, 2015).

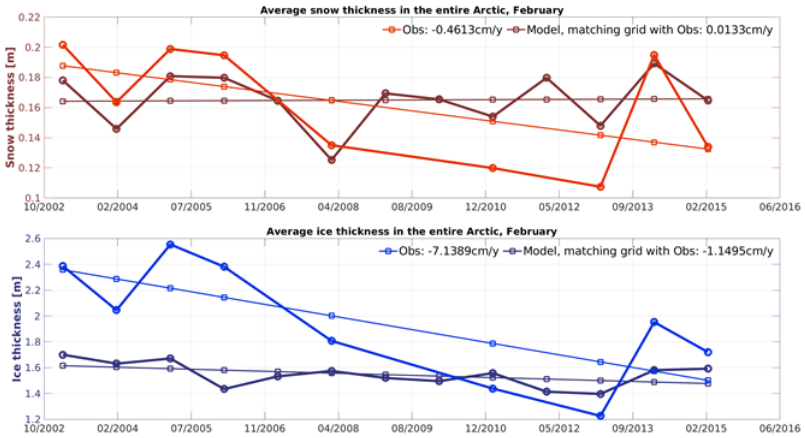

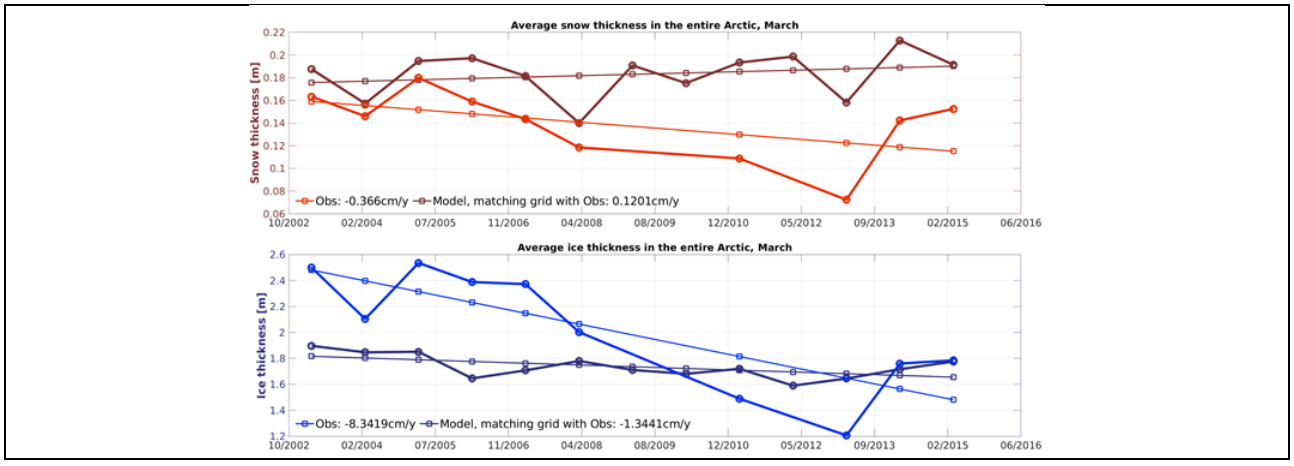

Figure 5 Modelled and observed time series and trends of snow depth (red'ish plots) and sea ice thickness (blue'ish plots) for the entire Arctic, for February (top panel) and March bottom panel.

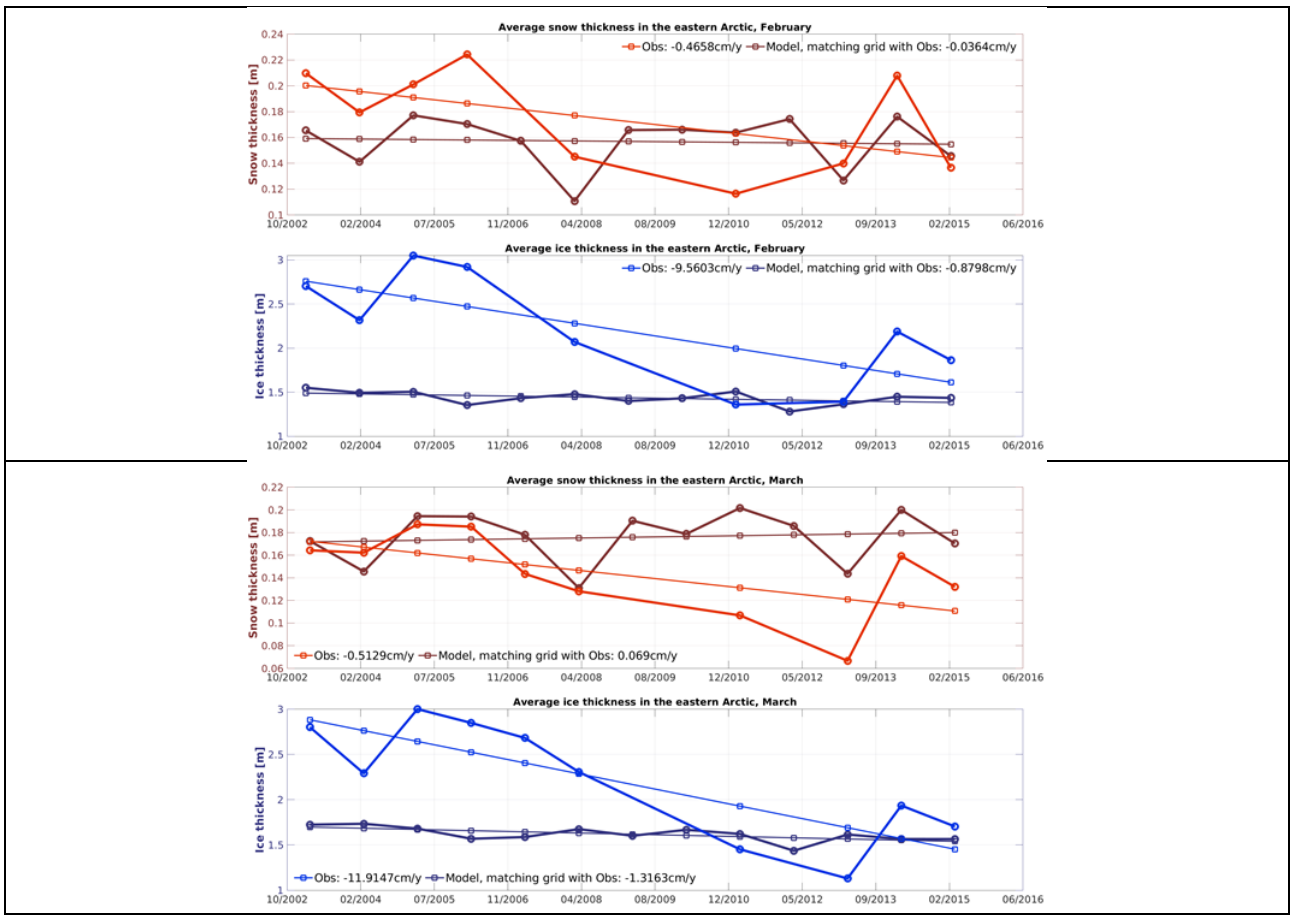

Figure 6 Modelled and observed time series and trends of snow depth (red'ish plots) and sea ice thickness (blue'ish plots) for Eastern Arctic, for February (top panel) and March bottom panel.

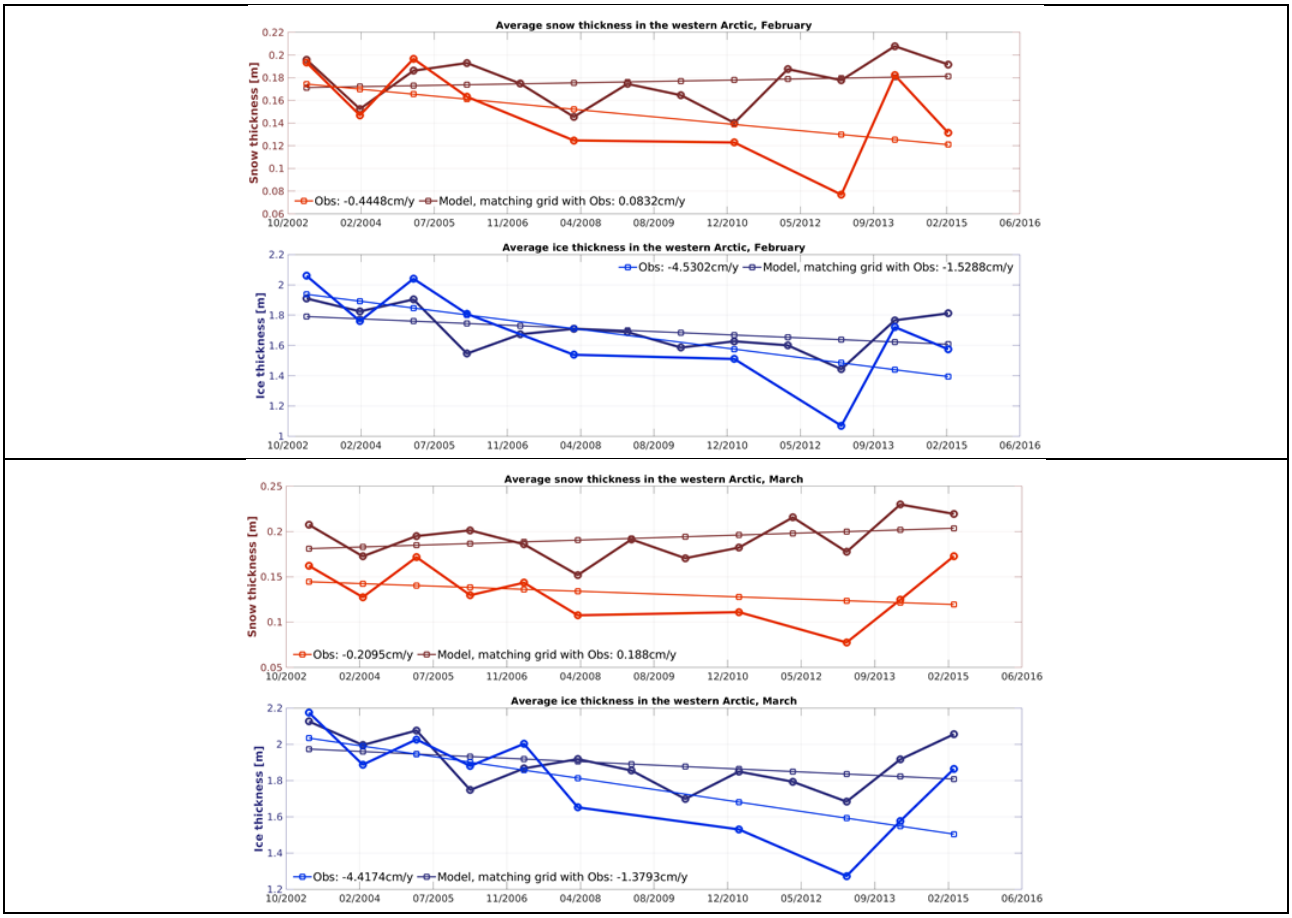

Figure 7 Modelled and observed time series and trends of snow depth (red'ish plots) and sea ice thickness (blue'ish plots) for Western Arctic, for February (top panel) and March bottom panel.

In figures 5, 6 and 7 the ice thickness time series of modelled and observed data show that the observed negative trends are much larger that the modelled in the 3 ice domains East, West and EA. Here the largest slope is consistently between the 2 major sea ice minima in 2017 and 2012, where large parts of the MYI was exported or melted. This is not reflected in the modelled ice thicknesses data set.

The snow depth estimated from model and observations do qualitative not agree. Observations estimate a negative trend in the winter month and a positive trend in November, whereas model data estimate very small trends with shifting signs.

The observed snow depth trends from February and March (mean) from this study is -4.1 mm/y, where another study calculated an Arctic snow depth trend of -2.9 mm/y, between 1950 and 2013, from ground and IceBridge observations (Webster et al., 2014). The corresponding trend from model data is -0.7 mm/y.

Despite a likely better agreement of the observation trends from this study with ground observation from the literature, it seems that the statistical snow depth performance of the model data is better that observations (see scatter plots).

6.4 Scatter plots

Two sets of scatter plots show modelled data and satellite data for March.
Figure 8 snow depth for the entire Arctic and for the Western and Easter sectors. A normalized histogram for both model and observation data indicate the mean and variance of each data set.

Model and observed snow depth have similar variance but different means. The predominantly FYI sector (East) show a model mean snow depth of approximately 18 cm and the corresponding observational mean is around 10 cm. Corresponding values for the MYI sector (West) 20 cm and 18 cm. Blanchard-Wrigglesworth (et al., 2018) showed from observations that mean April snow depth values for the period 2009-2015 for MYI and FYI are 25 cm and 30 cm, respectively. This indicates that the snow depth estimates from satellite observations are underestimated.

The scatter plots in Figure 9 show broad and realistic range of ice thickness in the observational data set and narrow ice thickness distribution in the modelled data set. The difference in modelled ice thickness mean between FYI and MYI is unrealistically low for both ice domains (Haas, 2017), emphasizing that the model representation of in particular MYI shall be revisited.

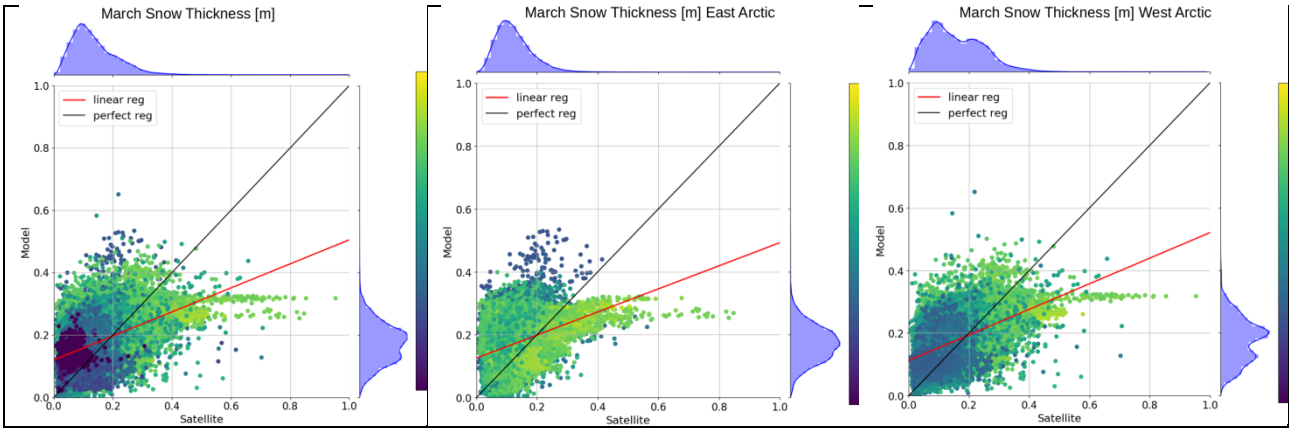

Figure 8 Snow Depth scatter plot comparing all data points from model (y-axis) with satellite data (x-axis) for the month of March. Colour bar shows Latitude and marginal density curves show distribution of the datasets. Black curve shows the 1:1 line and the red curve the actual linear regression for the data set. The normalized data histogram is plotted on each axis. Left panel show all Arctic, middle panel Eastern Arctic and right panel Western Arctic.

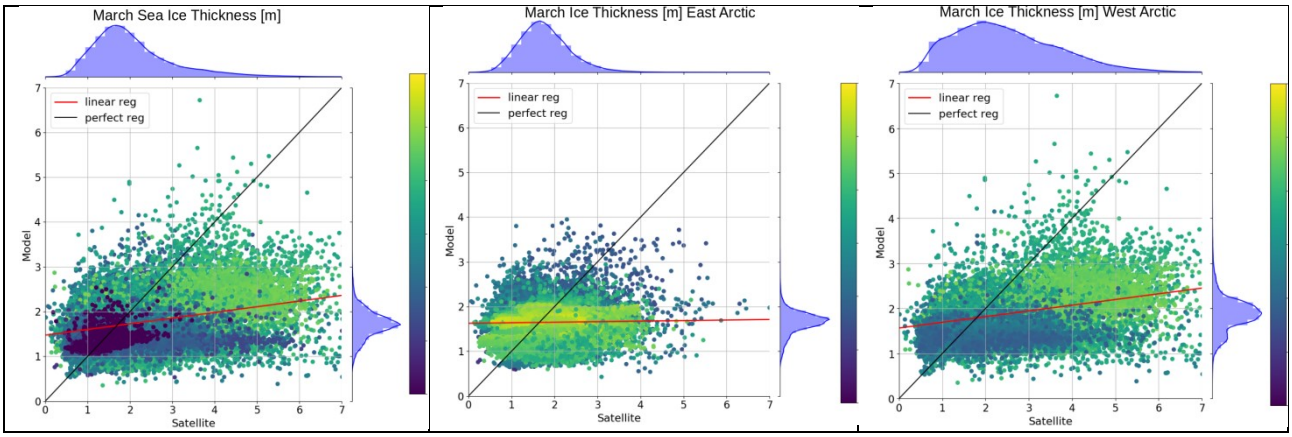

Figure 9 Sea Ice Thickness scatter plot comparing all data points at the same location from model (y-axis) and satellite data (x-axis) for the month of March. Colour bar shows Latitude and marginal density curves show distribution of the datasets. Black curve shows the perfect regression line and the red curve the actual linear regression for the data set. The normalized data histogram is plotted on each axis. Left panel show all Arctic, middle panel Eastern Arctic and right panel Western Arctic.

6.5 Trend maps

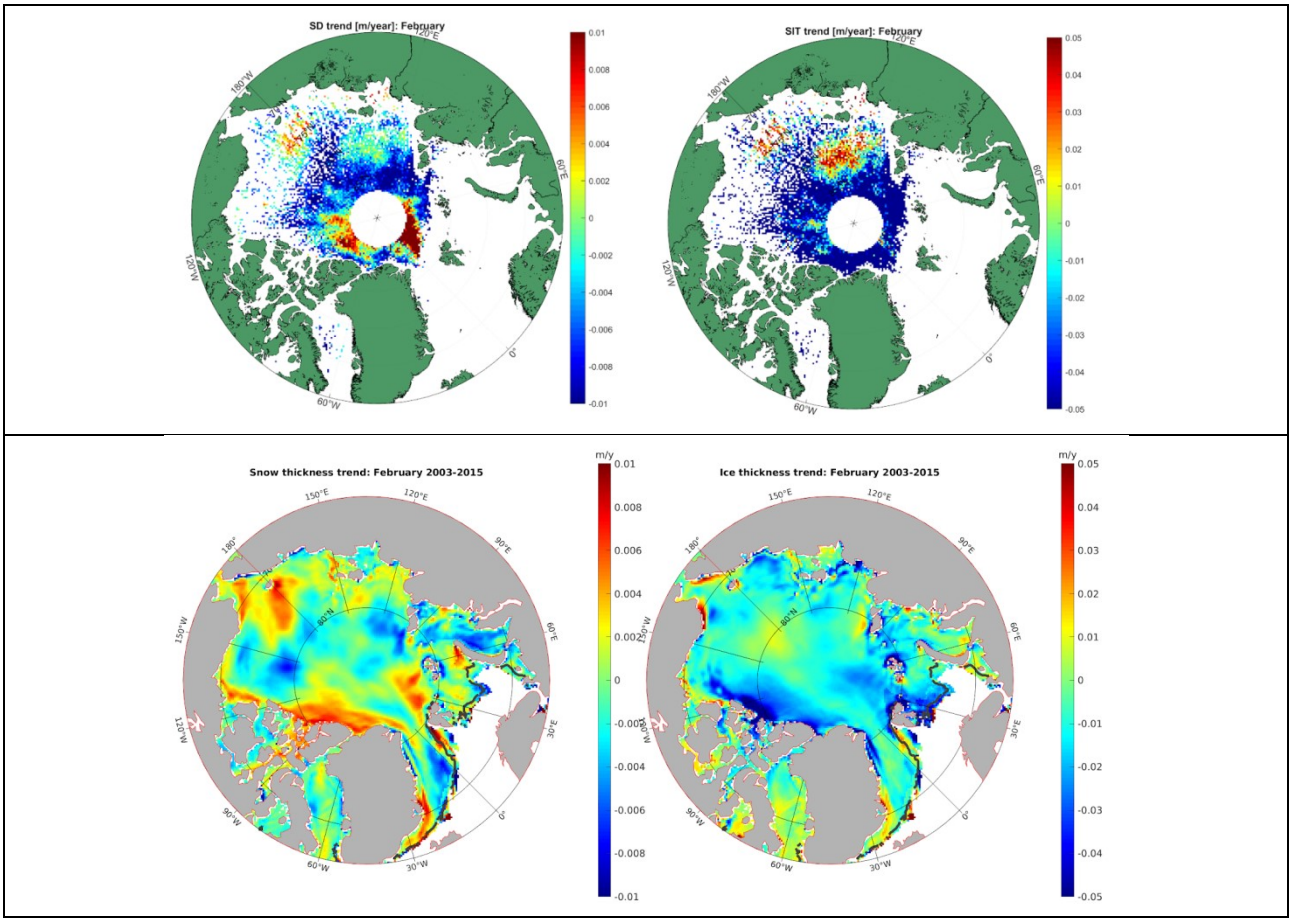

Figure 10 Snow and Ice thickness trends for February for the period 2003-2015. Satellite observations in the top panel, with snow thickness in the left maps and ice thickness in the right map. Likewise for model calculated snow and ice thickness trends in the bottom panel. The colour range from deep blue to deep red for -0.01 m/year to 0.01 m/year for snow thickness trends and from -0.05 m/year to 0.05 m/year for ice thickness trends, respectively.

Trend maps of snow depth and ice thickness in Figure 10 do not reveal much agreement between observation and model data. The maps represent February 2003-2015 as an example, as other show similar level of agreement. However, snow trends do agree qualitatively to some extent, with positive trends north of Svalbard, in the Laptev Sea and in the East Siberian Sea.

6.6 Ice and snow mean

The mean modelled and observed snow depth and ice thickness for the period 2003-2015 are very different.

As discussed above, the model melts nearly all Arctic sea ice over the summer, thus starting the ice formation from thin ice or open water at freeze-up in September/October. This means that the model has much thinner ice than the observations in those regions dominated by MYI north of Greenland and Canada and around the North Pole (Figure 11).

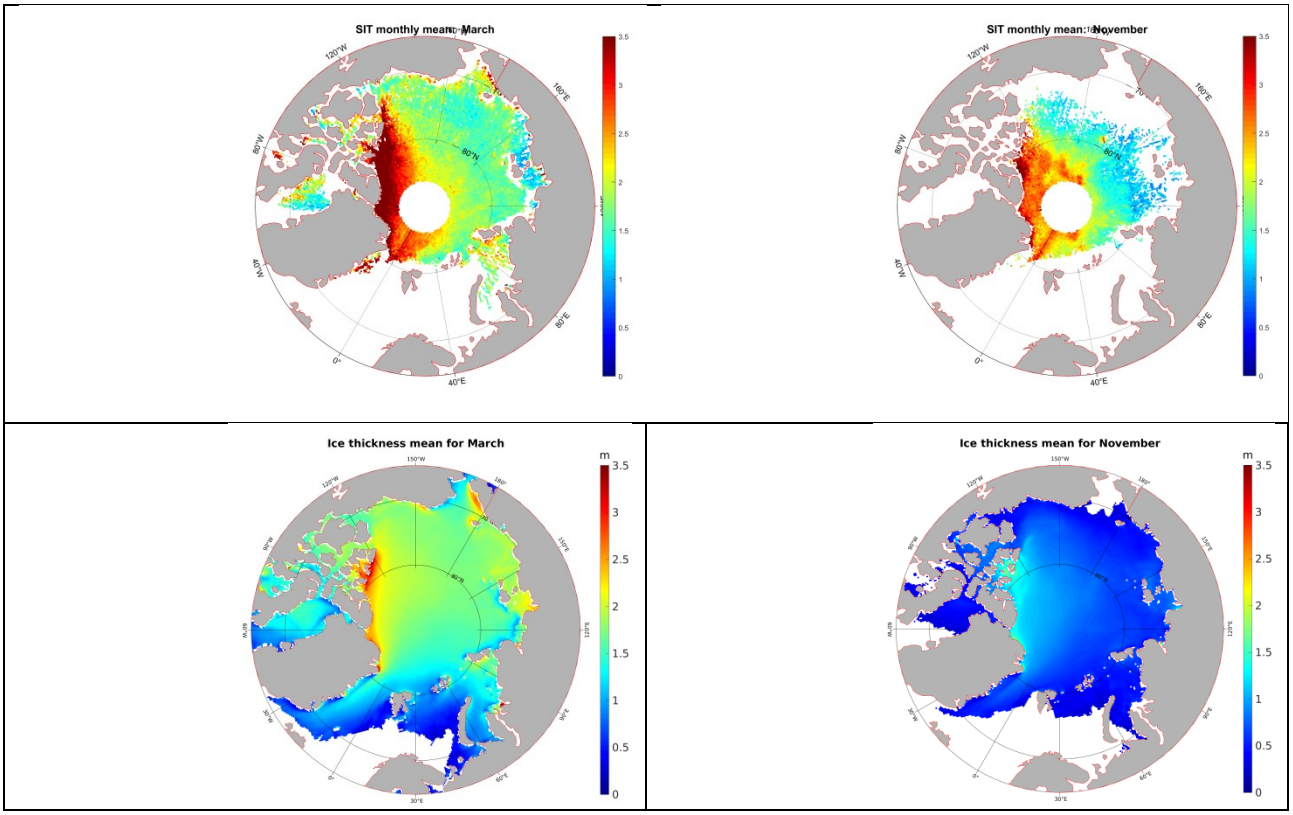

Figure 11 Mean sea ice thickness in March (left column) and November (right column) for the period 2003 to 2015. Observed thicknesses in row and modelled thicknesses in bottom row.

The mean snow thickness data do, like the observed and modelled sea ice thickness data, differ in both absolute values and in patterns in the month of March and November (Figure 12). The deep snow in the model in the Fram Straight in March is also reproduced in the observations but in the observations the deep snow extends across the North Pole and into the Lincoln Sea this is not seen in the model. In November the observed snow depth is up to 0.35 m in regions covered by MYI while the snow depth in the model is no more than 0.15 m. These differences between the model and the observations of snow depth are to some extent related to the “ice free” summers in the model. In some regions (North Pole region) the observed snow depth is decreasing from November to March while the modelled snow depth is increasing in all regions from November to March.

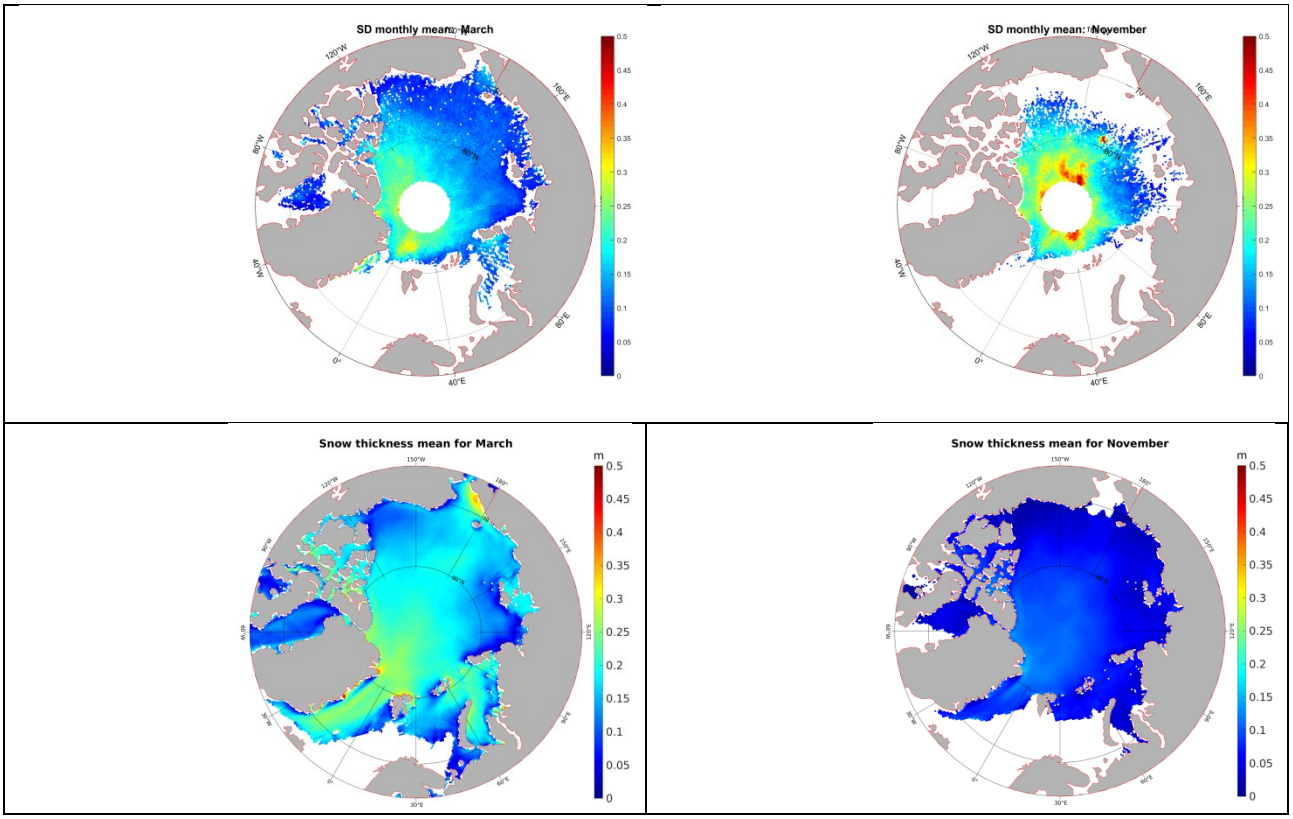

Figure 12 Mean snow depth in March (left column) and November (right column) for the period 2003 to 2015. Observed thicknesses in top row and modelled thicknesses in bottom row.

Mechanisms to decrease snow depth during the winter season is for example sublimation especially during wind redistribution events.

7 Conclusion

The modelled ice thickness trend is close to zero in the evaluated months of year (Nov., Feb., Mar.) and in the all selected sea ice domains (N80, EA, East, West), where the observed ice thickness trends are moderately to highly negative. The observed negative trends are in line with other observations reported in the literature. Melting of nearly all MYI in the model during summer is not observed and is the cause for many of the differences between the observed and modelled snow and ice thickness. Varying albedo or erroneous radiation budget in the model are candidates for this model flaw.

The ice thickness trends estimated from satellite reproduce trend estimates from the literature and the observed ice thickness time series reflect clearly the two extreme ice extent minima in 2007 and in 2012.

The observed snow depth and ice thickness does not necessarily increase over the winter months. This is counter intuitive at first sight, but not necessarily unrealistic due to ice dynamics, snow packing and snow drift. This should be investigated further.

Snow statistics (mean and variance) is in good agreement with other studies from the literature. In particular model snow mean values and variance is realistic, where the observed snow depth mean is slightly smaller than expected from other studies.

8 Future work

The authors have throughout the report identified issues to be looked into in future works. This is a recap of the most important issues.

In the ice thickness data that are retrieved by the alpha-method, it was found that mean ice thickness over large areas not always showed increasing thickness during the freezing period. This seems unlikely and should be investigated closer. The authors recommend looking into the radar penetration dependencies of e.g. snow salinity and density. We hope to find possible means to correct for annual variations of radar penetration depth that can improve ice thickness estimates. This will possible also lead to identifying differences between the radar penetration and emitting layer depth in FYI and MYI.

The alpha-method is also strongly depending on the derived alpha value. It is therefore advisable to continuously challenge the derived and applied alpha values by adding more snow observations to the data set and to continuously looking for possible temporal and spatial variations of alpha.

The modelled Arctic ice thickness offset in the beginning of the freezing period is very low, indicating that the surface energy balance in the ice module must be revisited. Tuning of model ice melt and freeze rates and albedo may solve an erroneous radiation budget in the model and it can possible lead to more realistic ice thicknesses and ice extent in the beginning of winter.

The initial state is important for forecasts of sea ice from short to medium range. Therefore, further comparison and ultimately assimilation of data should be investigated. In this context the most immediate variable to assimilate are snow and ice thickness and ice freeboard.

Finally, in the light of accelerating sea ice melt in the northern hemisphere it is crucial to update/extend the satellite time series to date from the current time series that terminates in 2015. From a climatological perspective the most recent years are of great importance for predictability of the Arctic sea ice status.

In short, the authors recommend focusing on following issues in future works.

- Evaluate radar penetration depth dependency to snow salinity and density.
- Enhance observation statistics for alpha calculation.
- Tuning of model ice melt and freeze rates and albedo.
- Assimilating satellite derived ice and snow parameters in ice model.
- Update satellite snow and ice thickness data set to 2020

9 References

Armitage, T. W. K., and Ridout, A. L.: Arctic sea ice freeboard from AltiKa and comparison with CryoSat-2 and Operation IceBridge, Geophys. Res. Lett., 42, 6724–6731, doi: 10.1002/2015GL064823, 2015.

Blanchard-Wrigglesworth, E., S. L. Farrell, T. Newman, and C. M. Bitz. Snow cover on Arctic sea ice in observations and an Earth System Model, Geophys. Res. Lett., 42, 10,342–10,348, doi: 10.1002/2015GL066049, 2015.

Blanchard-Wrigglesworth, E., Webster, M. A., Farrell, S. L., & Bitz, C. M. Reconstruction of snow on Arctic Sea Ice. Journal of Geophysical Research: Oceans, 123, 3588–3602, 2018.

CICE. https://cice-consortium-icepack.readthedocs.io/en/master/index.html, 2021.

CRREL. http://imb-crrel-dartmouth.org/, 2021

Dussin, R., Barnier, B., Brodeau, L., & Molines, J. M. The making of the Drakkar forcing set DFS5. *DRAKKAR/MyOcean Rep*, 01-04, 2016.

Dybkjær, G., and Eastwood, S.: Validation Report for the OSI SAF High Latitude L2 Sea and Sea Ice Surface Temperature, OSI-205, Version 1.1, OSI SAF, 30 pp., 2016.

Dybkjær, G., Eastwood, S., Borg, A. L., Højer, J., and Tonboe, R.: Algorithm theoretical basis document for the OSI SAF Sea and Sea Ice Surface Temperature L2 processing chain, OSI-205-a and OSI-205-b, Version 1.4, OSI SAF, 40 pp., 2018.

Dybkjær, G., Tonboe, R., Højer, J., and Eastwood, S.: Arctic and Antarctic snow and ice Surface Temperatures from AVHRR thermal Infrared satellite sensors, 1982-2015, 2020. (Manuscript in preparation).

GLORYS12. https://resources.marine.copernicus.eu/documents/PUM/CMEMS-GLO-PUM-001-030.pdf, 2021

Goldstein, M.A., A. H. Lynch, A. Chang and F. Fetterer. The step-like evolution of Arctic open water. Scientific Reports, 8:16902 | DOI:10.1038/s41598-018-35064-5, 2018.

Gurvan, M.; Romain Bourdallé-Badie; Jérôme Chanut; Emanuela Clementi; Andrew Coward; Christian Ethé; Doroteaciro Iovino; Dan Lea; Claire Lévy; Tomas Lovato; Nicolas Martin; Sébastien Masson; Silvia Mocavero; Clément Rousset; Dave Storkey; Martin Vancoppenolle; Simon Müeller; George Nurser; Mike Bell; Guillaume Samson Nemo Community model DOI 10.5281/zenodo.3838122, 2019.

Haas, C. Sea Ice, Chapter 2. Wiley Blackwell, Editor D.N Thomas. 3rd edition, 2017.

Hunke et al; CICE model; 10.5281/zenodo1205674, 2021.

Hunke, E. C and Dukowicz J. K. An Elastic-Viscous-Plastic model for Sea ice dynamics, Journal of Physical Oceanography, https://doi.org/10.1175/1520-0485(1997)027, 1997;

Japan Aerospace Exploration Agency (JAXA): Intercomparison results between AMSR2 and TMI/AMSR - E/GMI (AMSR2 Version 2.0), https://suzaku.eorc.jaxa.jp/GCOM_W/materials/product/150326_AMSR2_XcalResults.pdf, 2015. (Last access: 30 November 2020).

Kern, S., Khvorostovsky, K., Skourup, H., Rinne, E., Parsakhoo, Z. S., Djepa, V., Wadhams, P., and Sandven S.: The impact of snow depth, snow density and ice density on sea ice thickness retrieval from satellite radar altimetry: results from the ESA-CCI Sea Ice ECV Project Round Robin Exercise, The Cryosphere, 9, 37–52, doi: 10.5194/tc-9-37-2015, 2015.

Kim, J. M., Sohn, B. J., Lee, S. M., Tonboe, R. T., Kang, E. J., and Kim, H. C.: Differences between ICESat and CryoSat-2 sea ice thicknesses over the Arctic: Consequences for analyzing the ice volume trend. J. Geophys. Res.-Atmospheres, e2020JD033103., doi: 10.1029/2020JD033103

Karlsson, K.-G., Anttila, K., Trentmann, J., Stengel, M., Meirink, J. F., Devasthale, A., Hanschmann, T., Kothe, S., Jääskeläinen, E., Sedlar, J., Benas, N., van Zadelhoff, G.-J., Schlundt, C., Stein, D., Finkensieper, S., Håkansson, N., Hollmann, R., Fuchs, P., and Werscheck, M.: CLARA-A2: CM SAF cLoud, Albedo and surface RAdiation dataset from AVHRR data - Edition 2, Satellite Application Facility on Climate Monitoring (CM SAF), doi: 10.5676/EUM_SAF_CM/CLARA_AVHRR/V002, 2017.

Kurtz, N. T., and Farrell, S. L.: Large-scale surveys of snow depth on Arctic sea ice from Operation IceBridge, Geophys. Res. Lett., 38, L20505, doi:10.1029/2011GL049216, 2011.

Kurtz, N. T., Farrell, S. L., Studinger, M., Galin, N., Harbeck, J. P., Lindsay, R., Onana, V. D., Panzer, B., and Sonntag, J. G.: Sea ice thickness, freeboard, and snow depth products from Operation IceBridge airborne data, The Cryosphere, 7, 1035–1056., doi: 10.5194/tc-7-1035-2013, 2013.

Kurtz, N. T., Galin, N., and Studinger, M.: An improved CryoSat-2 sea ice freeboard retrieval algorithm through the use of waveform fitting, The Cryosphere, 8, 1217–1237, doi: 10.5194/tc-8-1217-2014, 2014.

Kurtz, N. and Harbeck, J.: CryoSat-2 Level-4 Sea Ice Elevation, Freeboard, and Thickness, Version 1, Boulder, Colorado USA. NASA National Snow and Ice Data Center Distributed Active Archive Center, doi: 10.5067/96JO0KIFDAS8, 2017.

Kwok, R. Arctic sea ice thickness, volume, and multiyear ice coverage: losses and coupled variability (1958–2018). Environ. Res. Lett. 13, 2018,

Kwok, R., Cunningham, G. F., Wensnahan, M., Rigor, I., Zwally, H. J., and Yi, D.: Thinning and volume loss of the Arctic Ocean sea ice cover: 2003–2008, J. Geophys. Res.-Oceans, 114(C7), C07005, doi: 10.1029/2009JC005312, 2009.

Kwok, R. and D. A. Rothrock. Decline in Arctic sea ice thickness from submarine and ICESat records: 1958–2008. GEOPHYSICAL RESEARCH LETTERS, VOL. 36, L15501, doi:10.1029/2009GL039035, 2009b.

Laxon, S., Peacock, N., and Smith, D.: High interannual variablility of sea ice thickness in the Arctic region, Nature, 425, 947–950, doi: 10.1038/nature02050, 2003.
Laxon, S. W., Giles, K. A., Ridout, A. L., Wingham, D. J., Willatt, R., Cullen, R., Kwok, R., Schweiger, A., Zhang, J., Haas, C., Hendricks, S., Krishfield, R., Kurtz, N., Farrell, S., and Davidson, M.: CryoSat-2 estimates of Arctic sea ice thickness and volume, Geophys. Res. Lett., 40, 732– 737, doi: 10.1002/grl.50193, 2013.

Lee, S.-M., and Sohn, B.-J.: Retrieving the refractive index, emissivity, and surface temperature of polar sea ice from 6.9 GHz microwave measurements: A theoretical development. J. Geophys. Res.-Atmos., 120, 2293-2305, doi: 10.1002/2014JD022481, 2015.

LINDSAY, R. W., J. Z HANG , A. S CHWEIGER , M. S TEELE , AND H. S TERN. Arctic Sea Ice Retreat in 2007 Follows Thinning Trend. JOURNAL OF CLIMATE VOLUME 22, 2009.

Lindsay, R., and A. Schweiger. Arctic sea ice thickness loss determined using subsurface, aircraft, and satellite observations. The Cryosphere, 9, 269–283, 2015.

Mallett, R. D. C., Lawrence, I. R., Stroeve, J. C., Landy, J. C., and Tsamados, M.: Brief communication: Conventional assumptions involving the speed of radar waves in snow introduce systematic underestimates to sea ice thickness and seasonal growth rate estimates, The Cryosphere, 14, 251-260, doi: 10.5194/tc-14-251-2020, 2020.

Maslanik, J., J.Stroeve, C. Fowler, and W. Emery. Distribution and trends in Arctic sea ice age through spring 2011. GEOPHYSICAL RESEARCH LETTERS, VOL. 38, L13502, doi:10.1029/2011GL047735, 2011.

Meier, W. N., Fetterer, F., Savoie, M., Mallory, S., Duerr, R., and Stroeve, J.: NOAA/NSIDC Climate Data Record of Passive Microwave Sea Ice Concentration, Version 3, Boulder, Colorado USA. NSIDC: National Snow and Ice Data Center, doi: 10.7265/N59P2ZTG, 2017.

OSISAF. http://www.osi-saf.org, 2020.

Ricker, R., Hendricks, S., Helm, V., Skourup, H., and Davidson, M.: Sensitivity of CryoSat-2 Arctic sea-ice freeboard and thickness on radar-waveform interpretation, The Cryosphere, 8, 1607–1622, doi: 10.5194/tc-8-1607-2014, 2014.

Rigor, Ignatius G., Roger L. Colony, and Seelye Martin. "Variations in surface air temperature observations in the Arctic, 1979–97." *Journal of Climate* 13.5, pp. 896-914, 2000.

Shi, H., Sohn, B.-J., Dybkjær, G., Tonboe, R. T., and Lee, S.-M.: Simultaneous estimation of wintertime sea ice thickness and snow depth from space-borne freeboard measurements, The Cryosphere, 14, 3761-3783, doi: 10.5194/tc-14-3761-2020, 2020.

Tiuri, M., A. Sihvola, E. Nyfors, and M. Hallikainen, The complex dielectric constant of snow at microwave frequencies, IEEE J. Ocean. Eng., 9, 377–382, 1984.

Ulaby, F. T., Moore, R. K., and Fung, A. K.: Microwave remote sensing: Active and passive, Volume 3 - From theory to applications, 1986.

Warren, S. G., Rigor, I. G., Untersteiner, N., Radionov, V. F., Bryazgin, N. N., Aleksandrov, Y. I., and Colony, R.: Snow depth on Arctic sea ice, J. Climate, 12(6), 1814–1829, doi: 10.1175/1520-0442(1999)012<1814:SDOASI>2.0.CO; 2, 1999.

Webster, M. A., I. G. Rigor, S. V. Nghiem, N. T. Kurtz, S. L. Farrell, D. K. Perovich, and M. Sturm, Interdecadal changes in snow depth on Arctic sea ice, J. Geophys. Res. Oceans, 119, 5395–5406, doi:10.1002/2014JC009985, 2014.

Wingham, D. J., Francis, C. R., Baker, S., Bouzinac, C., Brockley, D., Cullen, R., Chateau-Thierry, P., Laxon, S. W., Mallow, U., Mavrocordatos, C., Phalippou, L., Ratier, G., Rey, L., Rostan, F., Viau, P., and Wallis, D. W.: CryoSat: a mission to determine the fluctuations in Earth's land and marine ice fields, Adv. Space Res., 37(4), 841–871, doi: 10.1016/j.asr.2005.07.027, 2006.

Yi, D., and Zwally, H. J.: Arctic Sea Ice Freeboard and Thickness, Version 1., Boulder, Colorado USA. NASA National Snow and Ice Data Center Distributed Active Archive Center. doi: 10.5067/SXJVJ3A2XIZT, 2009.

H. Zuo, M. A. Balmaseda, S. Tietsche, K. Mogensen, and M. Mayer. The ECMWF operational ensemble reanalysis–analysis system for ocean and sea ice: a description of the system and assessment, Ocean Sci., 15, 779–808, https://doi.org/10.5194/os-15-779-2019, 2019.

Zwally, H. J., Schutz, B., Abdalati, W., Abshire, J., Bentley, C., Brenner, A., Bufton, J., Dezio, J., Hancock, D., Harding, D., Herring, T., Minster, B., Quinn, K., Palm, S., Spinhirne, J., and Thomas, R.: ICESat's laser measurements of polar ice, atmosphere, ocean, and land, J. Geodyn., 34, 405–445, doi: 10.1016/S0264-3707(02)00042-X, 2002.

Zygmuntowska, M., Rampal, P., Ivanova, N., and Smedsrud, L. H.: Uncertainties in Arctic sea ice thickness and volume: new estimates and implications for trends, The Cryosphere, 8(2), 705–720, doi: 10.5194/tc-8-705-2014, 2014.

10 Previous reports

Previous reports from the Danish Meteorological Institute can be found on:
https://www.dmi.dk/publikationer/